Blood First Edition Paper, prepublished online May 31, 2019; DOI 10.1182/blood.2018893404

American Society of Hematology
2021 L Street NW, Suite 900,
Washington, DC 20036
Phone: 202-776-0544 | Fax 202-776-0545
editorial@hematology.org

EFL1 mutations impair eIF6 release to cause Shwachman-Diamond syndrome

Tracking no: BLOOD/2018/893404R2

Shengjiang Tan (University of Cambridge), Laëtitia Kermasson (Institut IMAGINE UMR1163), Angela Hoslin (MRC Mammalian Genetics Unit, Harwell, UK), Pekka Jaako (University of Gothenburg), Alexandre Faille (Cambridge Institute for Medical Research, Cambridge, UK), Abraham Acevedo-Arozena (Hospital Universitario de Canarias), Etienne Lengline (Hopital Saint-Louis APHP), Dana Ranta (Department of Haematology, CHU de Nancy, Nancy, France), Maryline Poirée (CHU l'Archet), Odile Fenneteau (Hôpital Robert Debré APHP), Hubert Ducou le Pointe (Radiology Department, Armand Trousseau Hospital, APHP Paris, Paris, France), Stefano Fumagalli (Institut Necker Enfants Malades (INEM)), Blandine Beaupain (HOPITAL TROUSSEAU), Patrick Nitschké (Paris Descartes University), Christine Bôle-Feysot (INSERM UMR 1163, Genomics platform, Paris Descartes-Sorbonne Paris Cité University, Imagine Institut), Jean-Pierre de Villartay (INSERM Unite 768), Christine Bellanné-Chantelot (Pitié-Salpétrière Hospital, APHP), Jean Donadieu (Hopital Trousseau Assistance Publique des Hopitaux de Paris), Caroline Kannengiesser (Assistance publique-hôpitaux de Paris, Bichat), Alan Warren (University of Cambridge), and Patrick Revy (Imagine Institute for Genetic Diseases)

Abstract:
Shwachman-Diamond syndrome (SDS) is a recessive disorder typified by bone marrow failure and predisposition to hematological malignancies. SDS is predominantly caused by deficiency of the allosteric regulator SBDS that cooperates with the GTPase EFL1 to catalyze release of the ribosome anti-association factor eIF6 and activate translation. Here, we report biallelic mutations in EFL1 in three unrelated individuals with clinical features of SDS. Cellular defects in these individuals include impaired ribosomal subunit joining and attenuated global protein translation as a consequence of defective eIF6 eviction. In mice, Efl1 deficiency recapitulates key aspects of the SDS phenotype. By identifying biallelic EFL1 mutations in SDS, we define this leukemia predisposition disorder as a ribosomopathy that is caused by corruption of a fundamental, conserved mechanism, which licenses entry of the large ribosomal subunit into translation.

Conflict of interest: No COI declared

COI notes:

Preprint server: No;

Author contributions and disclosures: C.K. and P.R. initiated the project and performed whole exome sequencing analysis. P.R. and A.J.W. supervised, and coordinated the project. C.K., M.P., B.B., E.L., J.D., D.R. and C.B.C. identified affected patients or assisted with related clinical, genetic, and laboratory studies. Sanger sequencing and cloning were performed by L.K., B.C.B, C.K., and P.R. EFL1 constructs were generated by P.R. L.K. performed transduction of the wild type EFL1 expression vectors. A. F. and S.T. devised and performed ex vivo eIF6 release assays. A.A., A.H., P.J. and A.J.W. generated and performed phenotypic analyses of the Efl1 mutant mice. S.T. performed functional characterization of patient cell lines. P.R. and A.J.W. prepared figures, and wrote the manuscript supported by S.T., C.K., J.D., C.B.C., E.L., J-P.dV, P.J., A. F. and A.A.

Non-author contributions and disclosures: No;

Agreement to Share Publication-Related Data and Data Sharing Statement: Agreement to share publication-related data via emails to the corresponding author

Clinical trial registration information (if any):

EFL1 mutations impair eIF6 release to cause Shwachman-Diamond syndrome

Shengjiang Tan[1-3, #], Laëtitia Kermasson[4,5, #], Angela Hoslin[6, #], Pekka Jaako[1-3], Alex Faille[1-3], Abraham Acevedo-Arozena[6,7], Etienne Lengline[8], Dana Ranta[9], Maryline Poirée[10], Odile Fenneteau[11], Hubert Ducou le Pointe[12,13], Stefano Fumagalli[14], Blandine Beaupain[15], Patrick Nitschké[16], Christine Bôle-Feysot[17], Jean-Pierre de Villartay[4,5], Christine Bellanné-Chantelot[18], Jean Donadieu[19], Caroline Kannengiesser[20], Alan. J. Warren[1-3, *, †], Patrick Revy [4,5, *, †].

[1] Cambridge Institute for Medical Research, Keith Peters Building, Cambridge, UK
[2] Department of Haematology, University of Cambridge, Cambridge, UK
[3] Wellcome Trust–Medical Research Council Stem Cell Institute, University of Cambridge, Cambridge, UK
[4] INSERM UMR 1163, Laboratory of Genome Dynamics in the Immune System, Equipe Labellisée Ligue contre le cancer, Paris, France
[5] Paris Descartes–Sorbonne Paris Cité University, Imagine Institute, Paris, France
[6] MRC Mammalian Genetics Unit, Harwell, UK
[7] Unidad de Investigación, Hospital Universitario de Canarias, Instituto de Tecnologías Biomédicas ULL, and CIBERNED, La Laguna, Spain
[8] Department of Hematology, CRNMR Aplasie Médullaire, Saint-Louis University Hospital - AP-HP, Paris, France
[9] Department of Haematology, CHU de Nancy, Nancy, France
[10] Department of Pediatric Hematology-Oncology, CHU Lenval, Nice, France
[11] APHP, Laboratory of Hematology, Robert Debré University Hospital, Paris, France
[12] Radiology Department, Armand Trousseau Hospital, APHP Paris, Paris, France
[13] Department of Pediatric Imaging, Armand Trousseau Hospital, Sorbonne Universités, Pierre et Marie Curie-Paris University, Paris, France
[14] Institut Necker Enfants Malades (INEM), Paris, France; INSERM, U1151, Paris, France; Université Paris Descartes Sorbonne Cité, Paris, France
[15] French Neutropenia Registry, AP-HP Trousseau Hospital, Paris, France
[16] INSERM UMR 1163, Bioinformatics platform, Paris Descartes–Sorbonne Paris Cité University, Imagine Institute, Paris, France
[17] INSERM UMR 1163, Genomics platform, Paris Descartes–Sorbonne Paris Cité University, Imagine Institute, Paris, France; Genomic Core Facility, Imagine Institute-Structure Fédérative de Recherche Necker, INSERM U1163, Paris, France
[18] Department of Genetics, Hospital Pitié Salpétriére APHP, Sorbonne Université, Paris, France
[19] Service d'Hémato-Oncologie Pédiatrique, APHP Hôpital Trousseau, Registre des neutropénies - Centre de référence des neutropénies chroniques, Paris, France
[20] APHP Service de Génétique, Hôpital Bichat, Paris, France Université Paris Diderot, Sorbonne Paris Cité, Paris, France

# These authors equally participated to the work

* Co-senior authors

° Correspondence should be addressed to Patrick Revy (patrick.revy@inserm.fr) or Alan. J. Warren (ajw1000@cam.ac.uk)

Keywords: Shwachman-Diamond syndrome, ribosome, ribosomopathy, SDS, SBDS, EFL1, eIF6, bone marrow failure

Running title: EFL1 mutations cause Shwachman-Diamond syndrome

2 key points:

- Biallelic *EFL1* mutations cause Shwachman-Diamond syndrome

- EFL1 deficiency impairs eIF6 eviction from nascent 60S ribosomal subunits, reducing ribosomal subunit joining and attenuating protein synthesis

Abstract

Shwachman-Diamond syndrome (SDS) is a recessive disorder typified by bone marrow failure and predisposition to hematological malignancies. SDS is predominantly caused by deficiency of the allosteric regulator SBDS that cooperates with the GTPase EFL1 to catalyze release of the ribosome anti-association factor eIF6 and activate translation. Here, we report biallelic mutations in EFL1 in three unrelated individuals with clinical features of SDS. Cellular defects in these individuals include impaired ribosomal subunit joining and attenuated global protein translation as a consequence of defective eIF6 eviction. In mice, Efl1 deficiency recapitulates key aspects of the SDS phenotype. By identifying biallelic *EFL1* mutations in SDS, we define this leukemia predisposition disorder as a ribosomopathy that is caused by corruption of a fundamental, conserved mechanism, which licenses entry of the large ribosomal subunit into translation.

Introduction

Ribosomes are the essential macromolecular machines that carry out protein synthesis in all organisms. Eukaryotic ribosomes are formed by the association of the small 40S subunit (containing the 18S ribosomal RNA (rRNA)) and the large 60S subunit (containing the 28S, 5.8S, and 5S ribosomal RNAs (rRNAs)) to form actively translating 80S ribosomes[1]. In humans, mutations in the ribosome assembly factors or ribosomal proteins themselves lead to disorders termed ribosomopathies[2] that are associated with a range of clinical phenotypes including bone marrow failure, hematological malignancies and cancer[2-4].

Shwachman-Diamond syndrome (SDS) is an autosomal recessive disorder associated with bone marrow failure and an increased risk of progression to hematological malignancies including myelodysplastic syndrome (MDS) and acute myeloid leukemia (AML)[5]. SDS is also characterized by developmental anomalies including poor growth, exocrine pancreatic dysfunction, metaphyseal chondrodysplasia, and cognitive impairment[6,7]. In around 90% of cases, SDS is caused by biallelic mutations in the *SBDS* gene. Genetic, biochemical, and structural studies have revealed that the SBDS protein cooperates with elongation factor-like GTPase 1 (EFL1), a homolog of the ribosomal translocase elongation factor 2 (EF-2), during the terminal step in 60S subunit maturation to couple release of the ribosome anti-association factor eIF6 (yeast Tif6) to a final quality-control assessment of the integrity of the P-site and the GTPase center of the 60S subunit[4]. By binding to the sarcin-ricin loop and to ribosomal proteins uL3, uL14 and eL24 (using the new nomenclature[8]) on the intersubunit face of the 60S subunit, eIF6 forms a physical barrier to ribosomal subunit joining[4,9,10] and must therefore be removed to activate translation. However, an alternative model posits that protein kinase C (PKC) and the receptor for activated protein C (RACK1) promote eIF6 eviction through phosphorylation of eIF6 on residue S235[11].

Around 10% of individuals with SDS lack mutations in the *SBDS* gene. The identification of biallelic mutations in *DNAJC21* (yeast Jjj1) in a subset of SDS patients lacking mutations in the *SBDS* gene[12-15] indicates that SDS is genetically heterogeneous. Jjj1 cooperates with the cytoplasmic zinc-finger protein Rei1 (human ZNF622) to stimulate the ATPase activity of the Hsp70 chaperone Ssa

(human HSPA8), liberating the nuclear export factor Arx1 (human PA2G4) from its binding site near the peptide exit tunnel on the 60S subunit[16-20]. These data raise the possibility that additional components of the 60S subunit assembly pathway might also be mutated in SDS.

Here, we report the identification of biallelic mutations in the *EFL1* gene in individuals with clinical features of SDS. We demonstrate that disease-associated *EFL1* mutations disrupt eIF6 release from late cytoplasmic 60S subunits, thereby impairing ribosomal subunit joining and attenuating global translation. Furthermore, we show that *Efl1*-mutant mice recapitulate key aspects of the SDS phenotype. We define SDS as a ribosomopathy that is caused by corruption of a fundamental, conserved mechanism, which licenses the entry of the large ribosomal subunit into translation.

Materials and Methods

Patients. Informed consents were obtained from the families in accordance with the Declaration of Helsinki. This study was approved by the Institutional Review Board of INSERM and Assistance Publique des Hôpitaux de Paris.

Cell culture. Detailed procedure is described in Supplementary data.

Immunoblotting. Immunoblotting procedure is detailed in detailed in Supplementary data. Antibodies are listed in Supplementary Table 3.

Whole exome sequencing. Whole exome sequencing procedure is detailed in Supplementary data.

Targeted resequencing by NGS. Detailed procedure is described in Supplementary data.

cDNA analysis. Information on cDNA analysis is provided in Supplementary data.

Constructs. The *EFL1* open reading frame was PCR amplified and cloned into the lentiviral vectors p.lenti7.3/V5 TOPO (Invitrogen) and pCW57-GFP-P2A (Plasmid #71783; Addgene) for complementation experiments.

Measurement of protein synthesis. Measurement of protein synthesis, detailed in Supplementary data was performed as described[22].

Sucrose density gradients. Ribosomal subunits were separated by sucrose density gradients as described[23,24]. Detailed information is provided in **Supplemental Data.**

Cell fractionation. Detailed procedure is described in **Supplementary data.**

eIF6 release assay. Detailed information is provided in **Supplemental Data.**

EFL1 cloning, expression, and purification. Human EFL1 mutants were generated by PCR using the wild-type EFL1 cDNA (long isoform ENST00000268206.11). Detailed procedures are available **in supplementary data**.

Statistics. Student's t test (two-tailed, type two) was used to determine significant differences. $P < 0.05$ was considered significant.

Mice. Detailed procedure is described in **Supplementary data**.

Data sharing statement

For original data, please contact either patrick.revy@inserm.fr or ajw1000@cam.ac.uk.

RESULTS

Identification of biallelic *EFL1* mutations in three unrelated individuals

In the course of a systematic survey of individuals presenting with inherited bone marrow failure syndrome (IBMFS), we performed whole exome sequencing (WES) analysis to identify rare biallelic variants predicted to be pathogenic (frequency less than 0.1% in 1000 genomes, EVS, dbSNP, and our in-house database (8319 individuals)). This approach identified a male (P1) carrying compound heterozygous mutations in the *EFL1* gene (HGNC: 25789; Entrez Gene: 79631) encoding elongation factor-like GTPase 1 (EFL1) **(Fig. 1a)**. Since EFL1 physically and functionally interacts with SBDS[4,23,24,30], we considered *EFL1* as a strong candidate gene. Sanger sequencing confirmed the presence of biallelic *EFL1* mutations, including a nonsense mutation causing a premature stop codon on one allele (c.2260C>T; p.R754*) inherited from his healthy mother and also present in his healthy sister (**Fig. 1a and Supplementary Fig. 1a**), and a missense mutation leading to an amino acid substitution (c.1514T>C; p.F505S) on the allele inherited from his unaffected father **(Fig. 1a and Supplementary Fig. 1a)**. *EFL1* cDNA sequencing in P1 suggested reduced abundance of the allele carrying the c.2260C>T; p.R754* mutation, consistent with partial nonsense mediated decay (NMD) (**Supplementary Fig. 1a)**.

In order to identify additional individuals potentially carrying biallelic *EFL1* mutations, we analyzed the *EFL1* gene by gene-targeted sequencing of a cohort of 30 individuals who were diagnosed clinically with SDS but lacked mutations in the *SBDS* gene. This approach identified an *EFL1* homozygous missense mutation (c.2908C>T; p.R970H) in a female (P2), born from a consanguineous family (**Fig. 1b**). Sanger sequencing confirmed the mutation and indicated that both parents and the healthy siblings were heterozygous for the mutant *EFL1* allele (**Fig. 1b and Supplementary Fig. 1b**). In addition, we identified a third female (P3) carrying a heterozygous *EFL1* missense mutation (c.2647T>G; p.C883G) (**Fig. 1c**). Sanger sequencing confirmed the mutation and indicated that it was inherited from her father and also carried by her healthy brother (**Fig. 1c and Supplementary Fig. 1c**). No other pathogenic exon-encoded variants were detected in individual P3. However, the near absence of detectable wild type *EFL1* mRNA transcripts from the 'normal' allele in P3's cells suggests a

noncoding defect in the allele inherited from her mother that affects EFL1 expression **(Fig. 1c, Zoom)**. Sequence analysis of genomic DNA (gDNA) and cDNA of a synonymous single nucleotide variant (SNV) present in a heterozygous state in the *EFL1* coding sequence (rs4725) from control, P3 and P3's mother confirmed the defective expression of one *EFL1* allele in both P3 and her mother (**Supplementary Fig. 2a**). Furthermore, immunoblotting analysis demonstrated reduced EFL1 protein expression in B-LCL lysates from the mother of P3 compared with control, confirming the genetic results (**Supplementary Fig. 2b**). Haplotype analysis of the *EFL1* locus in P3's family indicated that P3's brother, unlike his sister, inherited the wild type maternal *EFL1* allele (**Supplementary Fig. 2c**). However, whole *EFL1* gene sequencing did not identify obvious genetic variants that could explain the defective expression of *EFL1* from the maternal allele. Nonetheless, biochemical analysis confirmed a functional *EFL1* defect in individual P3 (see below).

The four identified *EFL1* mutations affected both the long (ENST00000268206.11) and short (ENST00000359445.7) *EFL1* isoforms. Furthermore, they were absent or extremely rare in the gnomAD Browser (**Supplementary Table 1**) and in-silico tools (SIFT[31]; Polyphen2[32], CADD[33]) and the ACMG standards[34] predicted the *EFL1* coding variants to be deleterious (**Supplementary Table 1**). Moreover, the three missense mutations affect highly conserved amino acids across species (**Fig. 1d)**. Interestingly, the EFL1 p.F505S mutation maps to a key functional dynamic interface between EFL1 domains II-III (**Fig. 1e,f**) that mediates EFL1 conformational change on the ribosome[4]. In yeast, mutations that map to the EFL1 domain II-III interface likely suppress mutations in the P-site loop of uL16 (RPL10) by promoting conformational changes similar to those undergone by eukaryotic EF-2 and EF-G during translocation[35]. Both the p.C883G and p.R970H missense mutations map to the interface between EFL1 domain IV (**Fig. 1e,f**) and the C-terminal domain III of SBDS (**Fig. 2**). In yeast, domain IV is essential for Efl1 function in vivo[35]. Based on these observations, we hypothesized that the p.F505S, p.R970H and p.C883G mutations impair EFL1 function and that there is a causal link between the *EFL1* mutations identified and the SDS phenotype.

Clinical features of EFL1-deficient individuals

P1 is a male from a French family (**Table 1**) who was born at term with a birth weight of 2,480

g (<3.0 percentile) and height 47 cm (3.0 percentile). He initially presented with unsteady gait. He sustained a spontaneous femoral fracture at 5 years of age and required surgical correction of severe genu valgum at 12 years of age. Metaphyseal chondrodysplasia was noted on X-ray at 13 years of age (**Supplementary Fig. 3a)**. At 17 years of age, he developed mild thrombocytopenia and subsequently progressive leukopenia with neutropenia and mild anemia (**Supplementary Fig. 3b)**. At 27 years of age, he developed chronic diarrhea, with reduced fat-soluble vitamins and fecal elastase, consistent with exocrine pancreatic dysfunction. He developed portal hypertension and splenomegaly secondary to liver cirrhosis. Despite mild intellectual impairment, he was able to perform daily work. At 31 years of age, the bone marrow trephine was hypocellular, with typical hyposegmented neutrophils observed in SDS[5,36] **(Table 1 and Supplementary Fig. 3c)**. No clonal cytogenetic abnormality was detected.

P2, a girl, is the third child in a consanguineous family of four (**Table 1**). She was born at 40 weeks of gestation with a birth weight of 2,640 g (2.5 centile), height 46 cm (1.7 centile) and a head circumference of 32.5 cm (6.8 centile). She presented at 13 months of age with failure to thrive, anorexia, moderately elevated liver enzymes, reduced zinc and vitamin A levels and mild iron deficiency anemia **(Table 1 and Supplementary Fig. 3b)**. Although anti-gliadin antibodies were positive at 8 months of age, they were later negative. At 18 months of age, ataxia and nystagmus were observed. She developed mild iron deficiency anemia (corrected with oral iron supplementation) and mild thrombocytopenia. At 3.8 years of age, she was neutropenic and thrombocytopenic (**Supplementary Fig. 3b**). In addition, exocrine pancreatic deficiency was noted, based on low fecal elastase and fat-soluble vitamins (A and E). Abdominal CT scan showed no evidence of pancreatic lipomatosis. Bone marrow examination revealed hyposegmented neutrophils **(Table 1 and Supplementary Fig. 3c)**. She failed to achieve developmental milestones. Her visual acuity was very low (2/10 of both eyes) due to severe myopia (with no associated retinal abnormalities). She had normal social behavior with a normal WISC IV test[37] at 10 years of age. However, her academic progress was delayed by 2 years at a Special School for the Blind. Although skeletal X-rays were normal, she exhibited growth delay due to deficiency of growth hormone (GH), which was introduced at the age of 11 years. From 8-11 years of age, her growth rate decreased from -1.8 SD to -3 SD (height 125 cm),

when GH therapy was initiated. Two years later, her height was 138 cm (- 2.7 SD), but puberty had not started.

P3, a girl, is a second child from a non-consanguineous French family (**Table 1**). The older child and the parents are healthy. Growth delay and femoral shortening was noticed in utero at 32 weeks of gestation. Following a caesarean section at 39 weeks gestational age due to an abnormal cardiac rhythm, her birth weight was 2,160 g (0.1 centile), height 45 cm (1.2 centile) and pectus carinatum and short limbs were noted. Severe neonatal anemia and thrombocytopenia with abnormal liver function tests (3 x normal value) were observed at day 2. Transfusion-dependent anemia persisted until 2 years of age (**Supplementary Fig. 3b**) with erythroblastopenia and hyposegmented neutrophils in the bone marrow **(Table 1 and Supplementary Fig. 3c)**. Pancreatic insufficiency was diagnosed at 3 months of age, with chronic diarrhea, reduced fecal elastase and fat-soluble vitamins (A and E). Due to persistent anorexia, a gastrostomy was performed at 8 months of age and is still present at 5 years of age. At 2 years of age, she became red cell transfusion independent. Growth retardation persisted with a height of 88 cm (-6 SD) at age 7 years. She has major skeletal defects involving the vertebrae, limbs and ribs, including metaphyseal chondrodysplasia (**Supplementary Fig. 3a**). She has good social skills but impaired cognitive development and is currently attending a Special School with 3 years delay.

In summary all three individuals (P1, P2, and P3) exhibited hematological abnormalities, short stature and exocrine pancreatic insufficiency consistent with the clinical diagnosis of SDS. However, all three individuals were negative for mutations in the *SBDS* gene.

Impaired eIF6 release and attenuated translation in cells from *EFL1*-mutant individuals

EFL1 cooperates with its cofactor SBDS to evict eIF6 from the nascent 60S ribosomal subunit during the terminal step in cytoplasmic maturation[4]. We therefore set out to obtain *in vivo* evidence for impaired eIF6 recycling, defective ribosomal subunit joining, and impaired global protein translation in cells from individuals carrying *EFL1* mutations. Immunoblotting revealed that EFL1 protein in cell lysates from P1 and P3's fibroblasts was reduced to 15 % and 5 % respectively of wild type levels (**Fig. 3a**). Thus, biallelic *EFL1* mutations in individual P1 reduced the expression and/or stability of the

encoded EFL1 protein. Importantly, the low abundance of EFL1 in P3's fibroblast lysates confirmed the sequencing results obtained from P3-derived *EFL1* cDNA (**Fig. 1a, zoom and Supplementary Fig. 2**). In contrast, the expression of EFL1 was not affected by the p.R970H mutation present in P2's fibroblasts (**Fig. 3a**). Similar findings were made in B-LCL lysates from the same individuals (**Fig. 3b**). Furthermore, the expression of additional factors involved in terminal cytoplasmic ribosomal maturation (NMD3, DNAJC21, PA2G4, eIF6, and SBDS) was unaffected in EFL1-deficient cells (**Fig. 3a,b**).

Next, we tested if *EFL1* mutations affect EFL1 function in ribosomal biogenesis. Consistent with a defect in ribosomal subunit joining, sucrose gradient centrifugation analysis of lysates from EFL1 mutant fibroblasts revealed an increased ratio of 60S:80S ribosomal subunits relative to control (**Fig. 3c,d**). The severity of the ribosomal subunit joining defect correlated with the level of residual EFL1 protein expression in P1 and P3's lysates (**Fig. 3a,b**). Although the expression of mutant EFL1 protein in P2's cells is similar to wild type, the increased 60S:80S ratio in these cells indicates that there is functional impairment of the mutant EFL1 protein.

In wild type cells, eIF6 binds to pre-60S ribosomal subunits in the nucleus and shuttles to the cytoplasm, where it is released during the terminal step in 60S subunit maturation. Thus, eIF6 is distributed between both the nuclear and cytoplasmic compartments. Compared with controls, the amount of eIF6 in the nucleus of EFL1 mutant fibroblasts was reduced by 70-80% (**Fig. 3e,f**), consistent with a role for human EFL1 in promoting efficient nuclear recycling of eIF6.

As ribosomal subunit joining is impaired in EFL1 mutant fibroblasts derived from all three patients, we anticipated that global protein synthesis would be attenuated in these cells. Indeed, protein synthesis was reduced in fibroblasts from P1 (62 %), P2 (50 %) and P3 (51 %) as assessed by *in vivo* incorporation of O-propargyl-puromycin (OP-Puro) (**Fig. 3g,h**)[22,40]. To further link this translational defect with the EFL1 mutations, we cloned the wild type *EFL1* coding sequence into a lentiviral vector and transduced the EFL1 mutant fibroblasts from P1 and P3. The ectopic expression of wild type EFL1 improved the translation rate in cells derived from P1 and P3 (**Fig. 3i,j**). Likewise, the inducible expression of wild type EFL1 in cells from P1, P2, and P3 (**Fig. 3k**) improved both the ribosomal subunit joining defect as assessed by the 60S:80S ratio following sucrose gradient centrifugation (**Fig.**

3l,m) and global translation (**Fig. 3n**), as assessed by incorporation of the methionine analog azidohomoalanine (AHA)[22]. Lastly, we assessed the functional impact of the EFL1 missense mutations identified in P1, P2 and P3 by biochemically reconstituting eIF6 release *ex vivo* from human pre-60S ribosomal subunits. We added recombinant human wild type or mutant EFL1 proteins together with SBDS and GTP to eIF6-loaded pre-60S subunits extracted from P3-derived human fibroblasts and monitored eIF6 removal by immunoblotting the "free" and "bound" fractions after pelleting the ribosomal subunits through a sucrose cushion (**Fig. 3o**). Recombinant wild type EFL1 efficiently triggered eIF6 release (**Fig. 3p**). The p.C883G EFL1 mutant identified in individual P3 did not significantly impair eIF6 release compared with wild type EFL1 (**Fig. 3p**), suggesting that the combined defects in the polysome profile (**fig. 3c,d**), eIF6 subcellular localization (**fig. 3e,f**) and translation (**fig. 3g,h**) observed in the cells from P3 are a consequence of the strong reduction in EFL1 protein expression (**Fig. 3a,b**). In sharp contrast, both the p.F505S and p.R970H EFL1 mutants identified in P1 and P2, respectively, yielded a markedly reduced amount of eIF6 in the free fraction compared with wild type, indicating that their ability to remove eIF6 is impaired (**Fig. 3p**).

We conclude from these results that the SDS-associated *EFL1* mutations that we have identified are hypomorphic and cause the SDS phenotype by impairing (not completely abrogating) eIF6 release from late cytoplasmic 60S ribosomal subunits, thereby disrupting ribosomal subunit joining and attenuating global protein synthesis.

Efl1-mutant mouse recapitulates the Shwachman-Diamond syndrome phenotype

To further assess the pathogenic effects of EFL1 mutations *in vivo*, we analyzed the *Efl1*-K983R mouse line (henceforth named *Efl1*$^{K983R/K983R}$) generated by *N*-ethyl-*N*-nitrosourea (ENU)-induced mutagenesis[26]. Although the mouse mutation was not identified in any of the patients, Efl1 residue K983 (human K976) is highly conserved **(Fig. 4a**) and lies within domain IV of EFL1, in close proximity to human residues R970 and C883 mutated in P2 and P3, respectively (**Fig. 1f**). Most importantly, similar to the mutations identified in P1 and P3, the p.K983R substitution in the mouse causes a reduction in EFL1 protein expression as determined by immunoblotting **(Fig. 4b,c)** while the

total levels of eIF6 and SBDS were unaffected (data not shown). At the functional level, the murine p.K983R mutation also increased the 60S:80S ratio (**Fig. 4d,e**) although the relative rate of protein synthesis was not significantly affected (**Fig. 4f**). We conclude that the mouse p.K983R mutation is a valid model in which to study the broad phenotypic effects of EFL1 loss of function.

Efl1$^{K983R/K983R}$ mice were born at a normal Mendelian ratio and did not show any obvious pathological abnormalities after necropsy, including analysis of pancreas, liver, skeletal muscle and brain. However, the mice exhibited a significant reduction in weight compared with wild type or *Efl1*$^{K983R/wt}$ mice **(Fig. 4g)**, due to a progressive decrease in fat mass accumulation (**Fig. 4h**). Although X-rays revealed no structural abnormalities of the skeleton in the *Efl1*$^{K983R/K983R}$ mice (data not shown), bone mass density was significantly reduced compared with wild type littermates at different ages (**Fig. 4i**). At the hematological level, compared with wild type mice, the bone marrow cellularity (**Fig. 5a**) as well as the frequency and absolute numbers of hematopoietic stem and progenitor cells (including pMegE, MkP and pGM/GMP progenitors[29]) were reduced in *Efl1*$^{K983R/K983R}$ mice (**Fig 5b, c and supplementary figure 4**). Additionally, we noticed a significant reduction in hemoglobin (**Fig. 5d**), platelet (**Fig. 5e**), and total white cell counts (**Fig. 5f**) in *Efl1* $^{K983R/K983R}$ mice.

Some of the *EFL1*-deficient individuals suffered from motor abnormalities and cognitive deficits, also present in the *Efl1*$^{K983R/K983R}$ mutant mice. Indeed, we identified gait abnormalities (**Fig. 5g**) and motor dysfunction (**Fig. 5h**) when compared with littermate controls. Moreover, working memory was also disrupted in *Efl1*$^{K983R/K983R}$ mice, as tested via Y maze habituation (**Fig. 5i**).

We conclude from these observations that *Efl1*$^{K983R/K983R}$ mutant mice recapitulate key aspects of the SDS phenotype, strongly supporting a causal role for EFL1 dysfunction in SDS.

DISCUSSION

In this study, we provide compelling evidence that recessive *EFL1* mutations cause SDS by impairing release of eIF6 from nascent cytoplasmic 60S ribosomal subunits, thereby disrupting ribosomal subunit joining and attenuating global protein synthesis. Taken together with previous work[23,24,30], our human genetic and biochemical data indicate that the release of eIF6 by the concerted action of EFL1 and its allosteric activator SBDS is a fundamental conserved mechanism that licenses the entry of functionally competent large ribosomal subunits into active translation. These data do not support a critical role for RACK1 and PKCβII in the eviction of eIF6 in mammalian cells through the phosphorylation of eIF6 residue S235 as previously proposed[11]. Indeed, the position of RACK1 on the head of the 40S subunit[41], the viability and normal growth of PKCβ null mutant mice[42] and the observation that the phylogenetically conserved eIF6 residues 1-224 are sufficient for eIF6 recycling *in vivo*[4] are inconsistent with such a model. Our work provides the most compelling evidence to date that SDS is a ribosomopathy that is caused by mutations in multiple components (*SBDS*, *EFL1* and *DNAJC21*) of a coherent pathway involved in cytoplasmic maturation of the 60S ribosomal subunit maturation.

Through our analysis, we identified an *EFL1* pseudogene (*EFL1P1;* Chromosome 15: 84,080,168-84,126,604) that is located 1.8 Mb distal to the *EFL1* gene and is directionally inverted (**Supplementary Fig. 5a**). This is striking because in 89% of cases, *SBDS* mutations arise from a gene conversion event due to recombination between *SBDS* and its pseudogene (*SBDSP*), located 5.8 Mb distally in an inverted orientation[43,44]. Thus, the c.1514T>C (p.F505S) mutation identified in P1 might arise from gene conversion due to recombination between *EFL1* and the *EFL1P1* pseudogene containing this sequence change (**Supplementary Fig. 5b,c**). The genetic analysis of *EFL1* is further challenged by the existence of a second *EFL1* pseudogene (*EFL1P2*) located on a distinct chromosome (Chromosome 4: 65,142,703-65,145,763), as well as several segmental duplications located on chromosomes 15 and Y (**Supplementary Table 2**). These numerous genomic sequences that are highly homologous to the *EFL1* gene may hamper the identification of pathological variants in *EFL1*. Furthermore, an uncharacterized genetic event in P3 has resulted in a profound reduction in *EFL1*

expression from the maternal allele (**Fig. 1a, zoom and Supplementary Fig. 2**)[45,46]. This observation suggests that analysis of the *EFL1* coding sequence in SDS patients who lack *SBDS* mutations may be insufficient to detect the genetic events leading to defective *EFL1* expression. We therefore recommend that *EFL1* mutation status and EFL1 protein expression should be routinely assessed in individuals with SDS lacking mutations in *SBDS* and *DNAJC21*.

During the course of our study, Stepensky et al. and Tan et al. investigated a total of six individuals carrying biallelic variants in the EFL1-encoding gene[47,48]. However, the pathological significance of these mutations remains unclear as introduction of the corresponding disease-related variants in yeast had no significant effect on cell fitness[47] and the functional impact of the reported EFL1 missense variants on human ribosome assembly and translation was not assessed[47,48].

Autosomal dominant mutations in *SRP54*, a key member of the cotranslational protein-targeting pathway, results in neutropenia associated with SDS-like features such as pancreatic insufficiency and short stature[49,50]. However, myeloid maturation arrest at the promyelocyte stage and the presence of prominent cytoplasmic vacuoles in the myeloid precursors are not typical of classical SDS. Thus, the mechanism underlying the neutropenia may differ in patients with *SRP54* mutations compared with that in typical SDS patients.

Structural, biochemical and genetic studies[4,23,24,30,51] support a cofactor-dependent conformational-switching mechanism for release of the anti-association factor eIF6 from the intersubunit face of the 60S subunit. This model proposes that SBDS drives the conformational equilibrium of EFL1 towards a high affinity state that effectively competes with eIF6 for an overlapping binding site on the sarcin-ricin loop of the 60S subunit to promote eIF6 displacement. Supporting this hypothesis, cells derived from individuals carrying *EFL1* mutations exhibit defects in eIF6 release and recycling, ribosomal subunit joining and protein translation that were corrected by expressing the wild type EFL1 protein (**Fig. 3**). The *EFL1* p.C883G (P3) and murine p.K983R (human K976) mutations appear to simply reduce EFL1 expression. However, the EFL1 p.R970H mutation (P2) that is expressed at wild type levels is functionally defective. Interestingly, like residues C883 and K970, K976 maps to the interface between EFL1 domain IV (essential for Efl1 function in vivo in yeast[35]) and the C-terminal

domain of SBDS (**Fig. 1f**), where it may potentially disrupt the allosteric activation of EFL1 by SBDS. Furthermore, the EFL1 variants p.M882K and p.R1095Q reported by Stepensky et al[47], map to this interface. The EFL1 p.F505S mutation (P1) is also functionally impaired, likely disrupting a key dynamic interface between EFL1 domains II-III that mediates EFL1 conformational change on the ribosome[4]. However, further investigations are required to precisely delineate the underlying mechanisms.

We reinforce these data by characterizing a novel mouse model carrying a point mutation within the *Efl1* gene. Like the human *EFL1* mutations identified here, the EFL1 p.K983R mouse mutation leads to reduced EFL1 protein expression, resulting in defects in ribosomal maturation. The mutation models key aspects of the human disease, including hematological abnormalities and growth deficits, as well as the defects in motor and cognitive function that are also present in some of the patients identified here, strongly supporting the conclusion that the SDS phenotype is caused by loss of EFL1 function.

How do we explain the striking tissue proclivity in SDS? Our data demonstrate that similar to SBDS deficiency[30,38,39], impaired EFL1 function markedly attenuates global protein synthesis by impairing ribosomal subunit joining due to the reduced availability of free cytoplasmic 60S ribosomal subunits. Therefore, the SDS phenotype likely reflects at least in part the impaired capacity of specific tissues to upregulate global protein translation at key time-points during development (and indeed postnatally) due to inefficient recruitment of nascent 60S subunits into the actively translating pool. Impaired translation re-initiation of complex mRNAs carrying upstream open reading frames may also contribute to the SDS phenotype[52].

Tissue-specific sensitivities to cellular stress responses evoked by altered ribosome homeostasis may not only contribute to the SDS disease phenotype[54] but may also potentially drive cancer progression by promoting the selection of compensatory mutations[55]. Thus, the somatic acquisition of biallelic *TP53* variants in SBDS-deficient hematopoietic stem and progenitor cells is associated with clonal progression and transformation to poor prognosis MDS[5,55]. Furthermore, recurrent acquired interstitial deletions of chromosome 20 in SDS bone marrow cells encompass the *EIF6* gene[56,57],

providing a potential mechanism that allows SDS cells to bypass the defect in ribosomal subunit joining by reducing the cellular dose of eIF6. Whether eIF6 deletion indeed modulates the risk of acquiring somatic *TP53* variants and progression to MDS and AML is an interesting question that will require careful clinical follow up of all genetic subgroups of SDS. Our data support the hypothesis that the development of small molecules that mimic the effect of *TIF6* suppressor mutations in yeast[30] may have therapeutic potential in SDS.

Conflict-of-interest disclosure: The authors declare no competing financial interests.

Acknowledgements

We thank the patients and their families for their contribution in this study. P.R. is grateful to Prof. Alain Fischer for discussions, advice, and support. We acknowledge the excellent technical assistance of Alicia Fernandes for generating B-LCL (CRB, Imagine Institute, Paris, France). We thank Drs. F. Fouyssac, N. Aladjidi, V. Barlogis, and F. Monpoux for patient care. P.J. was funded by the Swedish Research Council (2014-06807). This work has been supported by institutional grants from INSERM, Ligue Nationale contre le Cancer (Equipe Labellisée La Ligue), and GIS-Institut des maladies rares, and by State funding from the Agence Nationale de la Recherche under "Investissements d'avenir" program (ANR-10-IAHU-01). P.R. is a scientist from Centre National de la Recherche Scientifique (CNRS). The work was also supported by a Specialist Programme from Bloodwise (12048, to AJW), the UK Medical Research Council (MC_U105161083, to AJW, MC_UP_A390_1106 and 1330931 to AAA), a Wellcome Trust strategic award to the Cambridge Institute for Medical Research (100140), a core support grant from the Wellcome Trust and MRC to the Wellcome Trust-Medical Research Council Cambridge Stem Cell Institute, Ted's Gang and The Connor Wright Shwachman Diamond Project (to AJW) and the Cambridge National Institute for Health Research Biomedical Research Centre.

Author contributions. C.K. and P.R. initiated the project and performed whole exome sequencing analysis. P.R. and A.J.W. supervised, and coordinated the project. C.K., M.P., B.B., E.L., J.D., D.R. and C.B.C. identified affected patients or assisted with related clinical, genetic, and laboratory studies. Sanger sequencing and cloning were performed by L.K., B.C.B, C.K., and P.R. EFL1 constructs were generated by P.R. L.K. performed transduction of the wild type EFL1 expression vectors. A. F. and S.T. devised and performed ex vivo eIF6 release assays. A.A., A.H., P.J. and A.J.W. generated and performed phenotypic analyses of the *Efl1* mutant mice. S.T. performed functional characterization of patient cell lines. P.R. and A.J.W. prepared figures, and wrote the manuscript supported by S.T., C.K., J.D., C.B.C., E.L., J-P.dV, P.J., A. F. and A.A.

References

1. Warren AJ. Molecular basis of the human ribosomopathy Shwachman-Diamond syndrome. *Adv Biol Regul*. 2017;S2212-4926(17):30153-30157.
2. Ruggero D, Shimamura A. Marrow failure: a window into ribosome biology. *Blood*. 2014;124(18):2784-2792.
3. Yelick PC, Trainor PA. Ribosomopathies: Global process, tissue specific defects. *Rare Dis*. 2015;3(1):e1025185.
4. Weis F, Giudice E, Churcher M, et al. Mechanism of eIF6 release from the nascent 60S ribosomal subunit. *Nat Struct Mol Biol*. 2015;22(11):914-919.
5. Donadieu J, Fenneteau O, Beaupain B, et al. Classification of and risk factors for hematologic complications in a French national cohort of 102 patients with Shwachman-Diamond syndrome. *Haematologica*. 2012;97(9):1312-1319.
6. Dror Y, Donadieu J, Koglmeier J, et al. Draft consensus guidelines for diagnosis and treatment of Shwachman-Diamond syndrome. *Ann N Y Acad Sci*. 2011;1242:40-55.
7. Hashmi SK, Allen C, Klaassen R, et al. Comparative analysis of Shwachman-Diamond syndrome to other inherited bone marrow failure syndromes and genotype-phenotype correlation. *Clin Genet*. 2011;79(5):448-458.
8. Ban N, Beckmann R, Cate JH, et al. A new system for naming ribosomal proteins. *Curr Opin Struct Biol*. 2014;24:165-169.
9. Gartmann M, Blau M, Armache JP, Mielke T, Topf M, Beckmann R. Mechanism of eIF6-mediated inhibition of ribosomal subunit joining. *J Biol Chem*. 2010;285(20):14848-14851.
10. Klinge S, Voigts-Hoffmann F, Leibundgut M, Arpagaus S, Ban N. Crystal structure of the eukaryotic 60S ribosomal subunit in complex with initiation factor 6. *Science*. 2012;334(6058):941-948.
11. Ceci M, Gaviraghi C, Gorrini C, et al. Release of eIF6 (p27BBP) from the 60S subunit allows 80S ribosome assembly. *Nature*. 2003;426(6966):579-584.
12. Tummala H, Walne AJ, Williams M, et al. DNAJC21 Mutations Link a Cancer-Prone Bone Marrow Failure Syndrome to Corruption in 60S Ribosome Subunit Maturation. *Am J Hum Genet*. 2016;99(1):115-124.
13. Dhanraj S, Matveev A, Li H, et al. Biallelic mutations in DNAJC21 cause Shwachman-Diamond syndrome. *Blood*. 2017;129(11):1557-1562.
14. Bluteau O, Sebert M, Leblanc T, et al. A landscape of germ line mutations in a cohort of inherited bone marrow failure patients. *Blood*. 2018;131(7):717-732.
15. D'Amours G, Lopes F, Gauthier J, et al. Refining the phenotype associated with biallelic DNAJC21 mutations. *Clin Genet*. 2018.
16. Meyer AE, Hoover LA, Craig EA. The cytosolic J-protein, Jjj1, and Rei1 function in the removal of the pre-60 S subunit factor Arx1. *J Biol Chem*. 2010;285(2):961-968.
17. Demoinet E, Jacquier A, Lutfalla G, Fromont-Racine M. The Hsp40 chaperone Jjj1 is required for the nucleo-cytoplasmic recycling of preribosomal factors in Saccharomyces cerevisiae. *RNA*. 2007;13(9):1570-1581.
18. Hung NJ, Johnson AW. Nuclear recycling of the pre-60S ribosomal subunit-associated factor Arx1 depends on Rei1 in Saccharomyces cerevisiae. *Mol Cell Biol*. 2006;26(10):3718-3727.
19. Lebreton A, Saveanu C, Decourty L, Rain JC, Jacquier A, Fromont-Racine M. A functional network involved in the recycling of nucleocytoplasmic pre-60S factors. *J Cell Biol*. 2006;173(3):349-360.
20. Meyer AE, Hung NJ, Yang P, Johnson AW, Craig EA. The specialized cytosolic J-protein, Jjj1, functions in 60S ribosomal subunit biogenesis. *Proc Natl Acad Sci U S A*. 2007;104(5):1558-1563.
21. Schindelin J, Arganda-Carreras I, Frise E, et al. Fiji: an open-source platform for biological-image analysis. *Nat Methods*. 2012;9(7):676-682.
22. Signer RA, Magee JA, Salic A, Morrison SJ. Haematopoietic stem cells require a highly regulated protein synthesis rate. *Nature*. 2014;509(7498):49-54.
23. Finch AJ, Hilcenko C, Basse N, et al. Uncoupling of GTP hydrolysis from eIF6 release on the ribosome causes Shwachman-Diamond syndrome. *Genes Dev*. 2011;25(9):917-929.
24. Wong CC, Traynor D, Basse N, Kay RR, Warren AJ. Defective ribosome assembly in Shwachman-Diamond syndrome. *Blood*. 2011;118(16):4305-4312.

25. Liu H, Naismith JH. An efficient one-step site-directed deletion, insertion, single and multiple-site plasmid mutagenesis protocol. *BMC Biotechnol*. 2008;8:91.
26. Potter PK, Bowl MR, Jeyarajan P, et al. Novel gene function revealed by mouse mutagenesis screens for models of age-related disease. *Nat Commun*. 2016;7:12444.
27. Kilkenny C, Browne W, Cuthill IC, Emerson M, Altman DG, Group NCRRGW. Animal research: reporting in vivo experiments: the ARRIVE guidelines. *Br J Pharmacol*. 2010;160(7):1577-1579.
28. Joyce PI, McGoldrick P, Saccon RA, et al. A novel SOD1-ALS mutation separates central and peripheral effects of mutant SOD1 toxicity. *Hum Mol Genet*. 2015;24(7):1883-1897.
29. Pronk CJ, Rossi DJ, Mansson R, et al. Elucidation of the phenotypic, functional, and molecular topography of a myeloerythroid progenitor cell hierarchy. *Cell Stem Cell*. 2007;1(4):428-442.
30. Menne TF, Goyenechea B, Sanchez-Puig N, et al. The Shwachman-Bodian-Diamond syndrome protein mediates translational activation of ribosomes in yeast. *Nat Genet*. 2007;39(4):486-495.
31. Kumar P, Henikoff S, Ng PC. Predicting the effects of coding non-synonymous variants on protein function using the SIFT algorithm. *Nat Protoc*. 2009;4(7):1073-1081.
32. Adzhubei IA, Schmidt S, Peshkin L, et al. A method and server for predicting damaging missense mutations. *Nat Methods*. 2010;7(4):248-249.
33. Kircher M, Witten DM, Jain P, O'Roak BJ, Cooper GM, Shendure J. A general framework for estimating the relative pathogenicity of human genetic variants. *Nat Genet*. 2014;46(3):310-315.
34. Richards S, Aziz N, Bale S, et al. Standards and guidelines for the interpretation of sequence variants: a joint consensus recommendation of the American College of Medical Genetics and Genomics and the Association for Molecular Pathology. *Genet Med*. 2015;17(5):405-424.
35. Bussiere C, Hashem Y, Arora S, Frank J, Johnson AW. Integrity of the P-site is probed during maturation of the 60S ribosomal subunit. *J Cell Biol*. 2012;197(6):747-759.
36. Donadieu J, Beaupain B, Fenneteau O, Bellanne-Chantelot C. Congenital neutropenia in the era of genomics: classification, diagnosis, and natural history. *Br J Haematol*. 2017;179(4):557-574.
37. Baron IS. Test review: Wechsler Intelligence Scale for Children-Fourth Edition (WISC-IV). *Child Neuropsychol*. 2005;11(5):471-475.
38. Ball HL, Zhang B, Riches JJ, et al. Shwachman-Bodian Diamond syndrome is a multi-functional protein implicated in cellular stress responses. *Hum Mol Genet*. 2009;18(19):3684-3695.
39. Calamita P, Miluzio A, Russo A, et al. SBDS-Deficient Cells Have an Altered Homeostatic Equilibrium due to Translational Inefficiency Which Explains their Reduced Fitness and Provides a Logical Framework for Intervention. *PLoS Genet*. 2017;13(1):e1006552.
40. Liu J, Xu Y, Stoleru D, Salic A. Imaging protein synthesis in cells and tissues with an alkyne analog of puromycin. *Proc Natl Acad Sci U S A*. 2012;109(2):413-418.
41. Khatter H, Myasnikov AG, Natchiar SK, Klaholz BP. Structure of the human 80S ribosome. *Nature*. 2015;520(7549):640-645.
42. Bansode RR, Huang W, Roy SK, Mehta M, Mehta KD. Protein kinase C deficiency increases fatty acid oxidation and reduces fat storage. *J Biol Chem*. 2008;283(1):231-236.
43. Boocock GR, Morrison JA, Popovic M, et al. Mutations in SBDS are associated with Shwachman-Diamond syndrome. *Nat Genet*. 2003;33(1):97-101.
44. Chen JM, Cooper DN, Chuzhanova N, Ferec C, Patrinos GP. Gene conversion: mechanisms, evolution and human disease. *Nat Rev Genet*. 2007;8(10):762-775.
45. Narzisi G, Schatz MC. The challenge of small-scale repeats for indel discovery. *Front Bioeng Biotechnol*. 2015;3:8.
46. Bailey JA, Eichler EE. Primate segmental duplications: crucibles of evolution, diversity and disease. *Nat Rev Genet*. 2006;7(7):552-564.
47. Stepensky P, Chacon-Flores M, Kim KH, et al. Mutations in EFL1, an SBDS partner, are associated with infantile pancytopenia, exocrine pancreatic insufficiency and skeletal anomalies in aShwachman-Diamond like syndrome. *J Med Genet*. 2017;54(8):558-566.
48. Tan QK, Cope H, Spillmann RC, et al. Further Evidence for the Involvement of EFL1 in a Shwachman--Diamond-like Syndrome and Expansion of the Phenotypic Features. *Cold Spring Harb Mol Case Stud*. 2018;4(5):pii: a003046.

49. Carapito R, Konantz M, Paillard C, et al. Mutations in signal recognition particle SRP54 cause syndromic neutropenia with Shwachman-Diamond-like features. *J Clin Invest*. 2017;127(11):4090-4103.
50. Bellanne-Chantelot C, Schmaltz-Panneau B, Marty C, et al. Mutations in SRP54 gene cause severe congenital neutropenia as well as Shwachman-Diamond-like syndrome. *Blood*. 2018.
51. Senger B, Lafontaine DL, Graindorge JS, et al. The nucle(ol)ar Tif6p and Efl1p are required for a late cytoplasmic step of ribosome synthesis. *Mol Cell*. 2001;8(6):1363-1373.
52. In K, Zaini MA, Muller C, Warren AJ, von Lindern M, Calkhoven CF. Shwachman-Bodian-Diamond syndrome (SBDS) protein deficiency impairs translation re-initiation from C/EBPalpha and C/EBPbeta mRNAs. *Nucleic Acids Res*. 2016;44(9):4134-4146.
53. Khajuria RK, Munschauer M, Ulirsch JC, et al. Ribosome Levels Selectively Regulate Translation and Lineage Commitment in Human Hematopoiesis. *Cell*. 2018;173(1):90-103 e119.
54. Tourlakis ME, Zhang S, Ball HL, et al. In Vivo Senescence in the Sbds-Deficient Murine Pancreas: Cell-Type Specific Consequences of Translation Insufficiency. *PLoS Genet*. 2015;11(6):e1005288.
55. Lindsley RC, Saber W, Mar BG, et al. Prognostic Mutations in Myelodysplastic Syndrome after Stem-Cell Transplantation. *N Engl J Med*. 2017;376(6):536-547.
56. Pressato B, Valli R, Marletta C, et al. Deletion of chromosome 20 in bone marrow of patients with Shwachman-Diamond syndrome, loss of the EIF6 gene and benign prognosis. *British Journal of Haematology*. 2012;157(4):503-505.
57. Valli R, Pressato B, Marletta C, et al. Different loss of material in recurrent chromosome 20 interstitial deletions in Shwachman-Diamond syndrome and in myeloid neoplasms. *Mol Cytogenet*. 2013;6(1):56.

Figure Legends

Figure 1. Identification of *EFL1* mutations in three individuals with SDS. Family pedigrees and direct Sanger sequencing of the *EFL1* gene in individuals 1 (P1) **(a)**, 2 (P2) **(b)** and 3 (P3) **(c)**. Arrows indicate the position of the mutations. **(d)** Multiple sequence alignment of EFL1 proteins from representative species. Identical amino acids are shown in red with white characters; similar amino acids are in red character; blue frame represents similarity across groups. **(e)** Schematic of the domain architecture of human EFL1 showing the position of disease-associated mutations. Domains I-V are indicated; id, insertion domain (residues 424-502), distinguish EFL1 from other translational GTPases. **(f)** Mapping of SDS-associated mutations onto human EFL1 (pdb 5anc[4]), shown in ribbon representation. Domains are colored deep salmon (I), light orange (id, II), cyan (III) and light blue (IV). Residue K976 corresponds to K983 mutated in the ENU mutant mouse model (see below).

Figure 2. SDS-associated EFL1 mutations map to key functional interfaces. SBDS C-terminal domain, magenta, space-filling representation; EFL1, cyan; eIF6, yellow (pdb code 5anb), ribbon representation. EFL1 domains II, III and IV are indicated. EFL1 residues targeted by mutations that map to the interface with SBDS are encircled. Residues mutated in SDS are indicated in black (this study) or red (Stepensky et al.[47]) text; residue K976 (cyan), targeted in the mouse model (this study). H69, rRNA helix 69.

Figure 3. SDS-associated *EFL1* mutations impair eIF6 release. (**a**) Total cell lysates from fibroblasts and (**b**) B-LCL from wild type (wt) and three individuals (P1, P2 and P3) with SDS were immunoblotted to visualize the indicated proteins. (**c**) Defective ribosome assembly in EFL1 mutant fibroblasts. Polysome profiles from fibroblast extracts from three unrelated individuals with SDS compared with wild type control. Quantification of the 60S:80S ribosomal subunit ratios is indicated as a bar chart (n≥5) (**d**). *EFL1* genotypes are provided in Suppl. Table 1. (**e**) EFL1 is required for eIF6 recycling in human cells. Indicated proteins were visualized by immunoblotting in cytoplasmic or nuclear fractions from wild-type and *EFL1* mutant fibroblasts. Histone H3, nuclear marker; HSP9, cytoplasmic marker. (**f**) Relative amount of eIF6 in the nucleus of *EFL1* mutant cells compared with wild type (n=5). (**g, h**) EFL1 deficiency attenuates protein synthesis. OP-Puro incorporation in fibroblast cells lines from individuals P1, P2 and P3 relative to wild type control cells quantified 1 hr after OP-Puro administration (n=6). (**i**) Complementation of EFL1-deficient fibroblasts with wild type EFL1. Lysates from *EFL1* mutant fibroblasts transduced with a vector expressing GFP alone (+ empty) or GFP + EFL1 (+EFL1) and from wild type (WT) fibroblasts as a control. The indicated proteins were visualized by immunoblotting. (**j**) Wild type EFL1 rescues global translation in patient fibroblast cell lines from P1 and P3 (n=4). **(k)** Complementation of EFL1-deficient fibroblasts with inducible vector allows wild type EFL1 expression after doxycycline (Dox) treatment. Lysates from EFL1 mutant fibroblasts transduced with an empty vector, or EFL1-expressing vector with (+) or without (-) Dox. Vinculin is used as a loading control. (**l**) Comparison of polysome profiles from wild type and *EFL1*-mutant fibroblasts transduced with empty vector or with inducible EFL1-expression vector treated (+) or not (-) with Dox. Arrows indicate increased 80S formation in complemented cells from individuals P1, P2 and P3**. (m)** Quantification of the 60S:80S ribosomal subunit ratios in cells transduced with inducible EFL1-expression vector treated (+) or not (-) with Dox (n=3). (**n**) Inducible expression of wild type EFL1 rescues global protein translation rates in EFL1-deficient fibroblast cell lines (n=6). (**o**) Schematic of eIF6 release assay. Pre-60S subunits extracted from P3-derived fibroblasts were incubated with the indicated release factors and pelleted through a 15% sucrose cushion. Immunoblotting reveals the eIF6 distribution in the supernatant ('free") and pellet ("bound"). (**p**) Release of eIF6 by SDS-associated EFL1 variants. P3-derived pre-60S subunits were incubated with GTP, SBDS and the indicated EFL1 variants. EDTA was added as a positive control for eIF6 release. eIF6 and uL14 were visualized by immunoblotting. (-) indicates the negative control lacking EFL1. All data represent mean ± s.e. Statistical significance between samples was assessed by two-tailed Student's t-test.

Figure 4. Efl1 K983R mutation leads to pleiotropic effects in mice. (**a**) Multiple sequence alignment of EFL1 proteins from representative species indicates that the murine EFL1 K983R mutation targets a

highly conserved residue. Identical amino acids are indicated by a red box with white characters; similar amino acids are in red characters; blue frame represents similarity across groups. (**b**) Representative total cell lysates of MEFs from wild type (*Efl1*$^{+/+}$), heterozygous *Efl1*$^{+/K983R}$ and homozygous *Efl1*$^{K983R/K983R}$ mice were immunoblotted to visualize EFL1 protein. GAPDH is used as a loading control. (**c**) Quantifications show the EFL1/GAPDH ratio. (**d**) Representative polysome profiles of MEF extracts from *Efl1*$^{K983R/K983R}$ (n=4) and heterozygous *Efl1*$^{+/K983R}$ (n=9) mice compared with wild type control (*Efl1*$^{+/+}$) (n=9). **(e)** Quantification of the 60S:80S ribosomal subunit ratios is indicated as a bar chart (n≥4). **(f)** Global protein translation rates in MEF from *Efl1* $^{K983R/K983R}$ and heterozygous *Efl1*$^{+/K983R}$ mice compared with wild type control (*Efl1*$^{+/+}$) (n=6). EFL1 K983R mutation reduces body weight from 3 weeks of age **(g)**, affecting the percentage of fat mass (**h**) and bone mass density (**i**) from 3 months of age. For all tests, p values are indicated.

Figure 5. Impaired hematopoiesis, motor abnormalities and cognitive deficits in *Efl1*$^{K983R/K983R}$ mice.
(**a**) Bone marrow cellularity in wild type and homozygous Efl1 $^{K983R/K983R}$ mice is indicated. (**b, c**) Frequencies of hematopoietic stem cells (HSC), megakaryocyte, granulocyte, erythroid progenitors (pMeGE), megakaryocyte progenitors (MkP), myeloid progenitors (preGM/GMP), and erythroid progenitors (pCFU-E and CFU-E) in the bone marrow in the indicated genotypes are shown (n=8 per genotype)[29]. EFL1 K983R mutation affects hematopoiesis. Hemoglobin levels (**d**), platelets (**e**), and total white blood cell counts (**f**). (**g**) Gait abnormalities in K983R mutant mice. Gait was analyzed using a qualitative scoring system at selected time points. Scores are explained in materials and methods. (**h**) Motor deficits in EFL1 K983R mutant mice. Free wheel running activity (over 7 nights, 3 months of age) for the indicated genotypes. (**i**) Cognitive deficits in K983R mutant mice. Y maze habituation testing of the indicated genotypes at 3 months of age. For all tests, p values are indicated.

Table

Table 1. Individuals with *EFL1* mutations meet clinical criteria for SDS.

Gender	M	F	F
Geographic origin	France	Africa Guinea	France
Consanguinity	No	Yes	No
Birth features	At term	At term	At term
Weight	2,840 (<3 percentile)	2,640 g (2.5 centile)	2,100 g (0.1 centile)
Height	47 cm (3 percentile)	46 cm (1.7 centile)	45 cm (1.2 centile)
Head circumference	NA	32.5 cm (6.8 centile)	NA
Evidence of bone marrow failure			
Initial manifestation and age at presentation	Thrombocytopenia, age 17 years	Failure to thrive, age 1.5 years	Anemia, failure to thrive age 1.2 months
Neutropenia	Mild	Severe	Mild
Absolute neutrophil count ($x10^9$/L). Median (min-max)	1.05 (1.0-3.9)	8.2 (1.0-37)	2.48 (1.83-4.0)
G-CSF	No	No	No
Red cell transfusion	No	No	Yes, during first year
Hemoglobin (g/L). Median (min-max)	118 (75-144)	104 (85-137)	114 (74 -182)
Thrombocytopenia	Severe	Mild	During follow up, thrombocytopenia ($51x10^9$/L) was observed only once, without hemorrhagic symptoms. Count recovered spontaneously.
Platelets ($x10^9$/L). Median (min-max)	32 (13-168)	110 (47-231)	201 (51-326)
Reticulocytes ($x10^9$/L)	109	72	73
MCV (fL)	90	94	103
HbF (%)	NA	5.8 (age 8 years)	NA
Platelet transfusion	No	No	No
Pancytopenia	Yes, after age 30 years	No	No
Bone marrow cellularity	Low (<5%). Two bone marrows (at age 28 years) reviewed. No myeloid maturation arrest. Segmentation defect in 8-22% of mature neutrophils.	Low. At age 8 years, no myeloid maturation arrest. Segmentation defect in 35% of mature neutrophils.	Normal in the first year of life, mildly decreased on the 3 bone marrow smears > 1 year old. Erythroblastopenia age 4 months. No myeloid maturation arrest age 5 years, no erythroblastopenia. Segmentation defect in 8% of mature neutrophils.
Bone marrow cytogenetics	Normal	Normal	Normal
Evidence of pancreatic dysfunction	Yes, age 27 years	Yes, age 5 years	Yes, age 6 months

Diagnosis of pancreatic insufficiency	Yes	Yes	Yes
Pancreatic enzyme therapy	Yes	Yes	Yes
Pancreatic MRI	Lipomatosis	No lipomatosis	No MRI, but hyper-echogenicity on US
Chronic diarrhoea	Yes	Yes	Yes
Faecal elastase	Low (<200 µg/g feces)	Low (< 200 µg/g feces)	Very low (<100 µg/g feces)
Vitamin A	Normal	Low	Low
Vitamin D	Normal	Normal	Normal
Vitamin E	NA	Normal	Normal
Liver	Portal hypertension with splenomegaly. Fibrosis evaluated on CT scan and liver biopsy age 29 years. Virology negative	Normal liver MRI. Elevated liver enzymes AST/ALT, (50-170 IU/L), then spontaneous recovery. No biopsy.	Normal liver MRI. Elevated liver enzymes AST/ALT, (60-120 IU/L). No biopsy.
Skeletal abnormalities	Claudication and atraumatic femoral neck fracture at 5 years of age.Severe osteoporosis, poly-epiphyseal and metaphyseal dysplasia with major bilateral genu valgum, patellar luxation, hip subluxation and bilateral oval femoral heads. Surgery for genu valgum complicated by osteitis, but outcome was favorable. Coxa plana and metaphyseal chondrodysplasia noted at age 29 years.	No abnormalities	Metaphyseal dysplasia.Skeletal defects of the vertebrae, limbs and ribs. Pectus carinatum
Bone density	Low, T score (vertebrae) -3.2 SD	Not evaluated	Not evaluated
Growth impairment	Short stature -2.6 SD. No therapy	Short stature -3 SD (not improved by pancreatic enzyme replacement). GH deficiency. GH therapy	Short stature -6 SD (not improved by pancreatic enzyme replacement). GH deficiency. No therapy
Eyes	Normal	Very severe myopia with low visual acuity	Normal
Ears	Normal	Hypoacusia	Normal
Cognitive impairment and developmental delay	Normal	Mild. 2 year delay at a special school for learning disabilities. Speech delay but at age 10 years, WISC- IV test[1] normal for age	Mild. 3 years delay in special school for learning disabilities.
Neurological symptoms	None	Ataxia. Nystagmus. CNS MRI normal but Chiari type I malformation diagnosed at 2 yrs	None. CNS MRI normal.

Dentition	Abnormal tooth enamel	Numerous dental caries	Normal
Skin abnormalities	No	No	No
Recurrent bacterial Infections	No	No	Yes
Age at last follow up	31 years	14 years	8 years
Vital status	Alive	Alive	Alive

Abbreviations:
HbF, hemoglobin F; MCV, red blood cell mean corpuscular volume; U/K, unknown; MRI, magnetic resonance imaging; CNS, central nervous system; WISC-IV (Wechsler Intelligence Scale for Children-Fourth Edition) test; AST, aspartate amino transferase; ALT, alanine aminotransferase; GH, growth hormone; SD, standard deviation; NA, not available; IU, international unit.

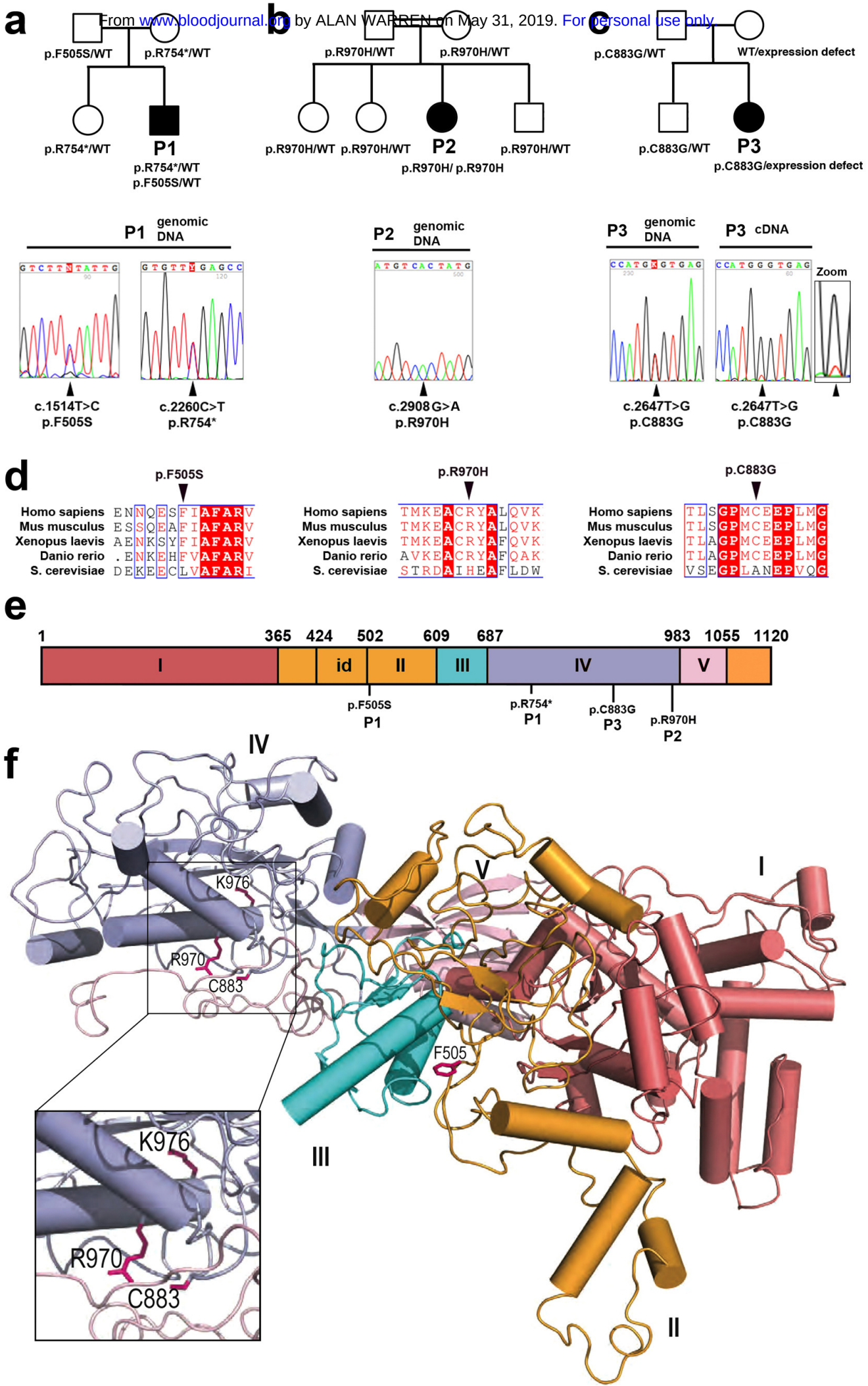

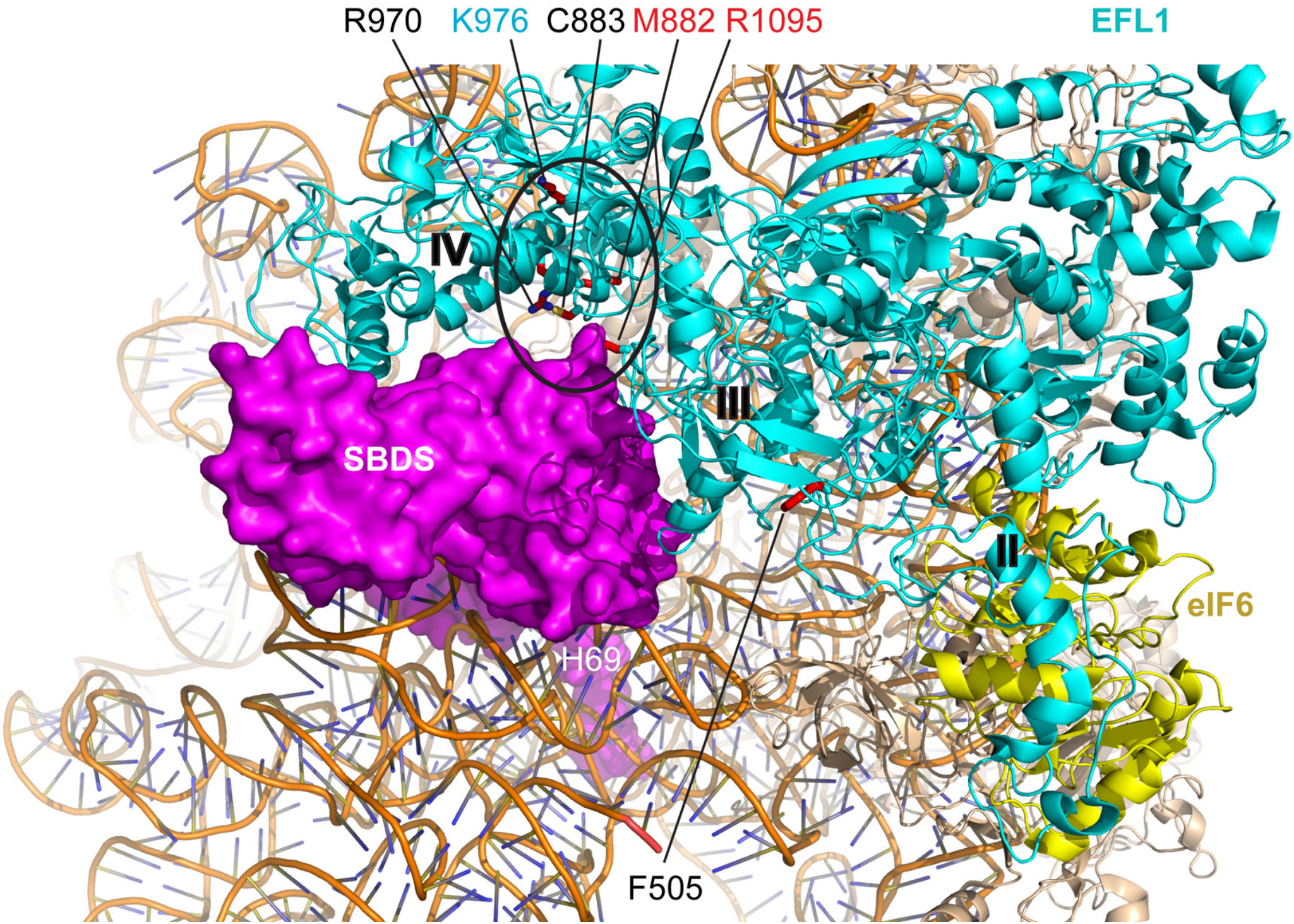
R970
K976
C883
M882
R1095
EFL1
IV
III
II
SBDS
H69
eIF6
F505

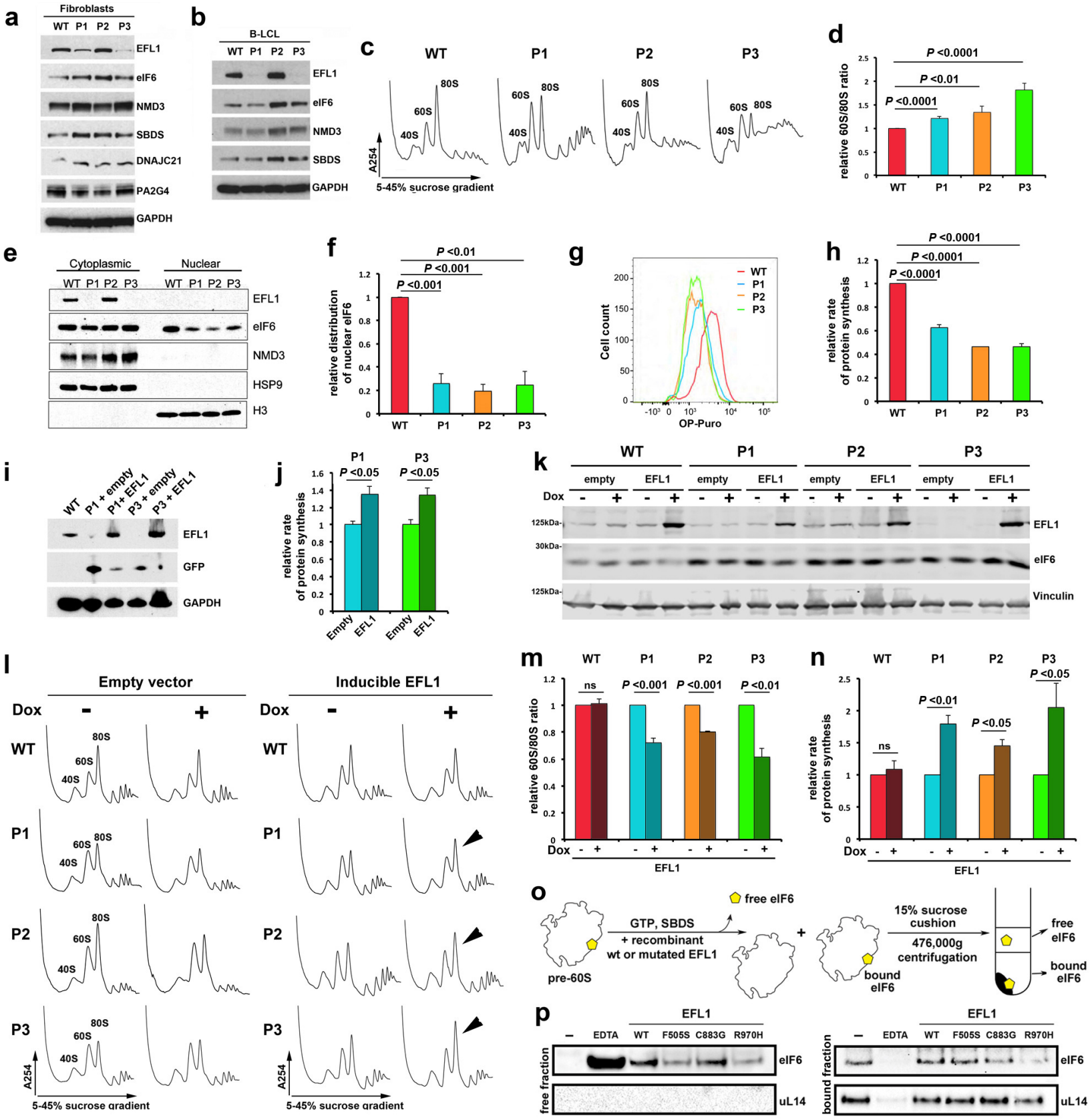

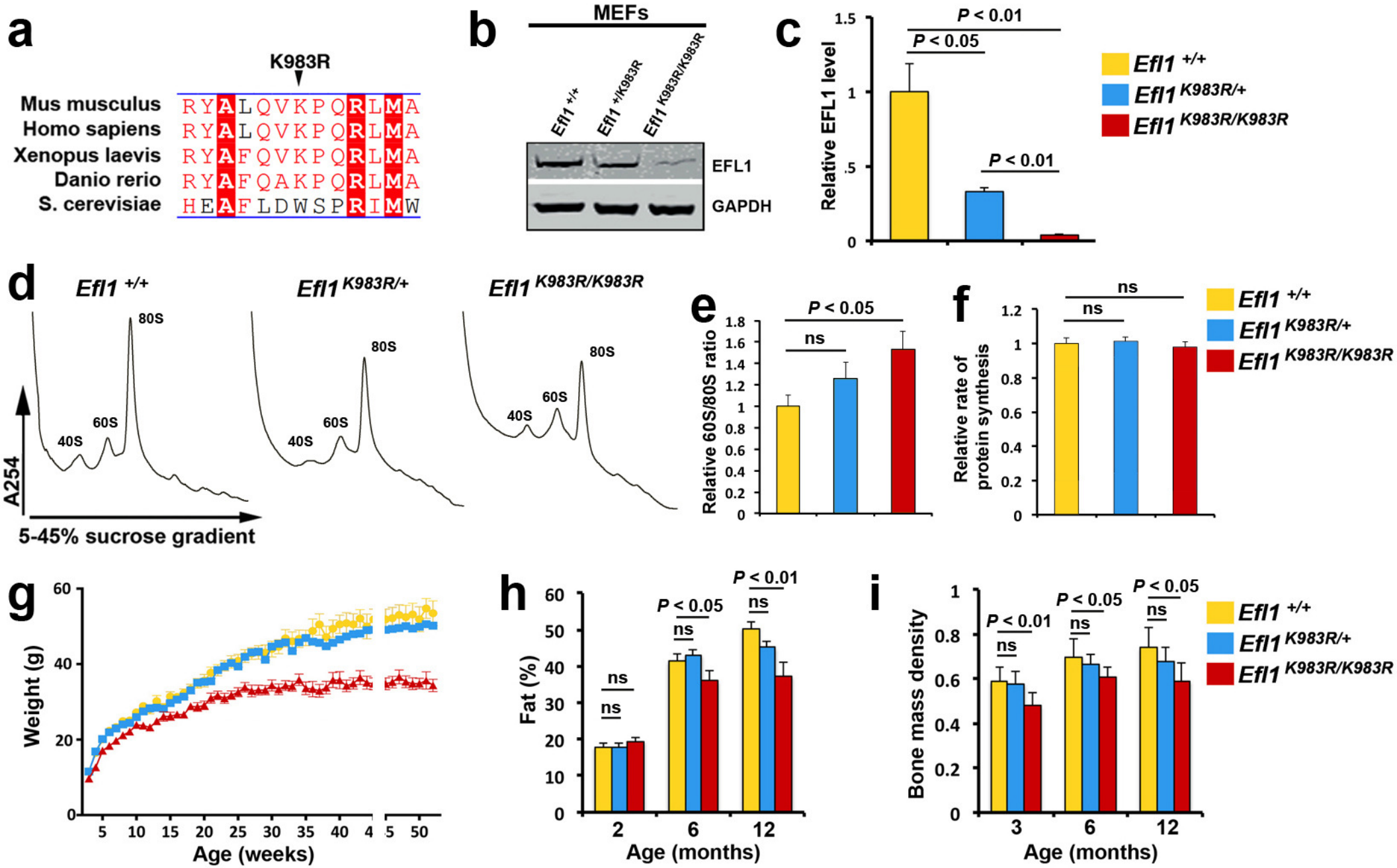
a
K983R
Mus musculus RYALQVKPQRLMA
Homo sapiens RYALQVKPQRLMA
Xenopus laevis RYAFQVKPQRLMA
Danio rerio RYAFQAKPQRLMA
S. cerevisiae HEAFLDWSPRIMW
b
MEFs
Efl1 +/+
Efl1 +/K983R
Efl1 K983R/K983R
EFL1
GAPDH
c
Relative EFL1 level
P < 0.01
P < 0.05
P < 0.01
Efl1 +/+
Efl1 K983R/+
Efl1 K983R/K983R
d
Efl1 +/+
Efl1 K983R/+
Efl1 K983R/K983R
80S
60S
40S
A254
5-45% sucrose gradient
e
Relative 60S/80S ratio
P < 0.05
ns
f
Relative rate of protein synthesis
ns
ns
g
Weight (g)
Age (weeks)
h
Fat (%)
P < 0.05
P < 0.01
ns
Age (months)
i
Bone mass density
P < 0.01
P < 0.05
P < 0.05
ns
Age (months)

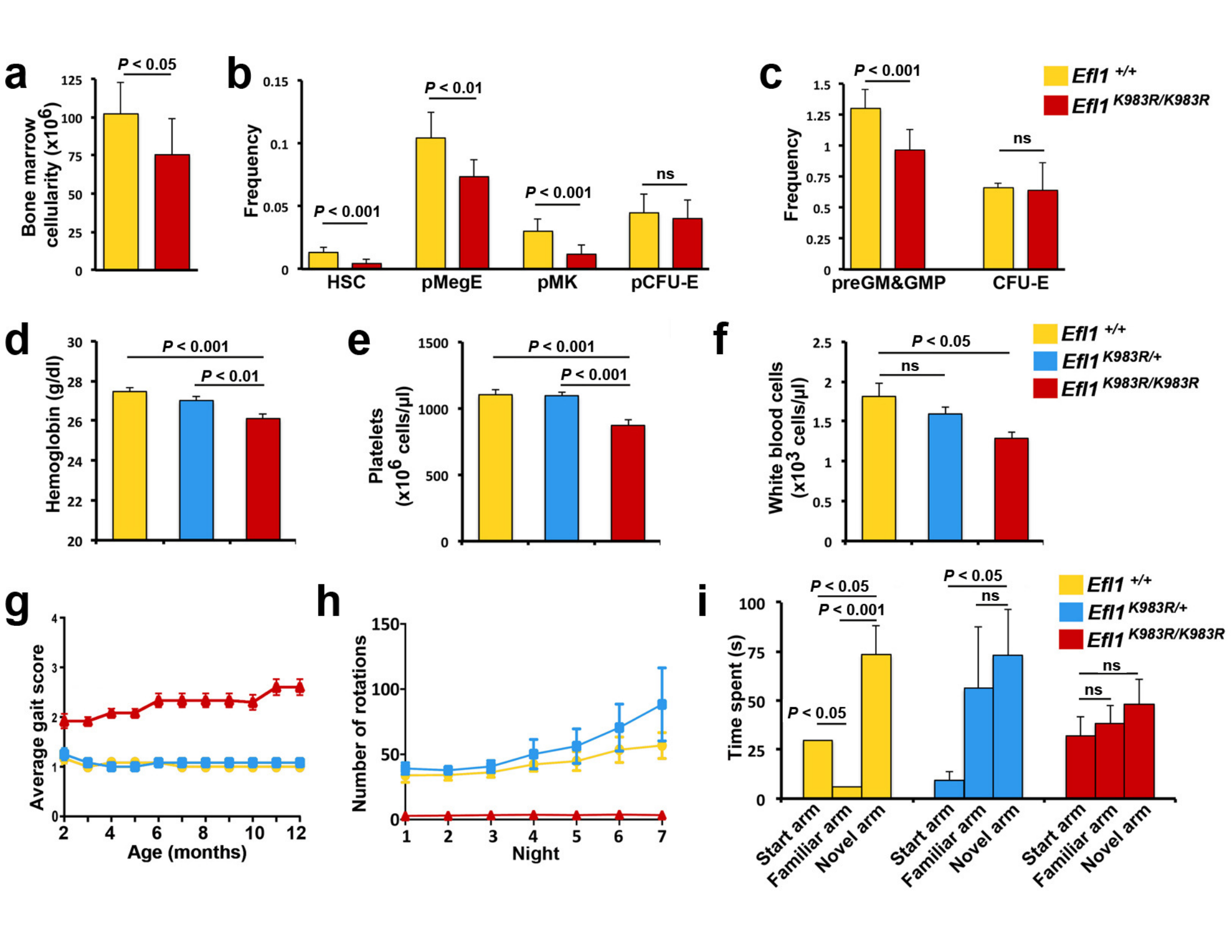
a
Bone marrow cellularity (x10^6)
P < 0.05
b
Frequency
P < 0.001
P < 0.01
P < 0.001
ns
HSC
pMegE
pMK
pCFU-E
c
Frequency
P < 0.001
ns
preGM&GMP
CFU-E
Efl1 +/+
Efl1 K983R/K983R
d
Hemoglobin (g/dl)
P < 0.001
P < 0.01
e
Platelets (x10^6 cells/µl)
P < 0.001
P < 0.001
f
White blood cells (x10^3 cells/µl)
P < 0.05
ns
Efl1 +/+
Efl1 K983R/+
Efl1 K983R/K983R
g
Average gait score
Age (months)
h
Number of rotations
Night
i
Time spent (s)
P < 0.05
P < 0.05
P < 0.001
P < 0.05
ns
ns
ns
Start arm
Familiar arm
Novel arm
Efl1 +/+
Efl1 K983R/+
Efl1 K983R/K983R

Prepublished online May 31, 2019;
doi:10.1182/blood.2018893404

EFL1 mutations impair eIF6 release to cause Shwachman-Diamond syndrome

Shengjiang Tan, Laëtitia Kermasson, Angela Hoslin, Pekka Jaako, Alexandre Faille, Abraham Acevedo-Arozena, Etienne Lengline, Dana Ranta, Maryline Poirée, Odile Fenneteau, Hubert Ducou le Pointe, Stefano Fumagalli, Blandine Beaupain, Patrick Nitschké, Christine Bôle-Feysot, Jean-Pierre de Villartay, Christine Bellanné-Chantelot, Jean Donadieu, Caroline Kannengiesser, Alan J. Warren and Patrick Revy

Blood (print ISSN 0006-4971, online ISSN 1528-0020), is published weekly by the American Society of Hematology, 2021 L St, NW, Suite 900, Washington DC 20036.